Parameter optimization and test of digging-shaking-pulling ginger harvesting device based on DEM-MBD coupled simulation

Fangyan Wang[1,2,3*], Fulun Tian[1], Wenlong Wang[1], Renchao Wang[1], Huan Zhang[1], Xin Wang[4*]

(1. *College of Mechanical and Electrical Engineering, Qingdao Agricultural University, Qingdao 266109, Shandong, China*;
2. *Collaborative Innovation Center for Shandong's Main Crop Production Equipment and Mechanization, Qingdao 266109, Shandong, China*;
3. *Shandong Provincial Key Laboratory of Smart Agricultural Equipment for Protected Horticulture, Qingdao 266109, Shandong, China*;
4. *College of Civil Engineering & Architecture, Qingdao Agricultural University, Qingdao 266109, Shandong, China*)

Abstract: The primary objective of this study was to address the challenges associated with the harvesting of ginger, namely the large resistance to digging, the high damage rate, and the high impurity rate of the harvested ginger. To this end, a digging-shaking-pulling ginger harvesting device (DSPGHD) was designed and optimized. The device was then analyzed in accordance with agronomic requirements for ginger planting and harvesting. This analysis involved the examination of interactions between ginger, soil, and mechanisms at each stage of the harvesting process. The study determined the key factors affecting the harvesting indices, including the initial angle of the clearing bar (IACB) φ, the length of the clearing bar (LCB) l_2, and the frequency of shaking (FS) f. The coupled EDEM-RecurDyn simulation system was established, and the key factors were tested with the forward resistance, the ginger force, and the effect of the soil flow as the test indices. A single-factor test was conducted, and the test result data was analyzed to determine the factor influence law. The field orthogonal test was then designed to optimize the parameter combinations of the device, and the response surface analysis and multi-objective optimization method were used to obtain better parameter combinations of the evaluation indices of ginger harvesting. These were as follows: the IACB was 8.7°, the LCB was 256 mm, and the FS was 4.24 Hz. The sizes of the test indices were as follows: the forward resistance was 1526 N, the damage rate was 4.57%, and the impurity rate was 3.74%. The DEM-MBD model developed in this study has the capacity to investigate the interactions between the primary factors of the DSPGHD and ginger-soil. It can optimize the geometric structure of the machine and provide a theoretical foundation for field trials. The optimized results from the field orthogonal test can satisfy the agronomic requirements and use requirements of ginger harvesting, and reduce the input of labor.

Keywords: DEM-MBD coupling, ginger, harvesting machinery, soil, digging and shaking and pulling
DOI: 10.25165/j.ijabe.20261901.9937

Citation: Wang F Y, Tian F L, Wang W L, Wang R C, Zhang H, Wang X. Parameter optimization and test of digging-shaking-pulling ginger harvesting device based on DEM-MBD coupled simulation. Int J Agric & Biol Eng, 2026; 19(1): 97–107.

1 Introduction

Ginger is a pivotal cash crop in China, occupying the foremost position in global terms of both planting area and production[1]. However, the mechanization rate remains low, with manual harvesting being the predominant practice. This has resulted in significant labor wastage and escalating planting costs. During the harvest season, the challenge of sourcing sufficient labor, coupled with the high cost of labor, poses a significant obstacle to the growth and advancement of the ginger industry[2,3]. Presently, the majority of domestic ginger harvesters are capable of only simple digging, exhibiting high digging resistance and stringent requirements for machine stability. Despite the recent advent of ginger combine harvesters, these machines remain in the experimental stage and do not align with the specific agronomic requirements of China's ginger harvest. Large-scale joint harvesting machines used in Europe and the United States are not designed to meet the specific challenges posed by Chinese ginger cultivation conditions. As ginger planting benefits are enhanced and the scale of planting is expanded, there is an urgent need for a multifunctional harvesting device that can perform the functions of digging, soil clearing, clamping, and conveying to meet the operational needs of integration at this stage. However, there is a paucity of research on ginger digging, shaking, and pulling harvesting technology and theory, and mature ginger harvesting equipment is scarce[4]. The digging-shaking-pulling ginger harvesting device (DSPGHD) studied in this paper can effectively reduce the digging resistance, damage rate, and impurity rate of the ginger harvesting machine, which is of great significance for increasing the machine harvesting rate of ginger, reducing the planting cost, and promoting the development of the ginger industry in China.

The discrete element simulation technique is a highly promising numerical simulation method for the design and optimization of agricultural machinery. This has led to a substantial

Received date: 2025-05-26 **Accepted date:** 2025-11-20
Biographies: **Fulun Tian**, MS candidate, research interests: agricultural machinery and equipment, Email: tianfulun2023@163.com; **Wenlong Wang**, MS candidate, research interests: agricultural machinery and equipment, Email: 1315378398@qq.com; **Renchao Wang**, MS candidate, research interests: agricultural machinery and equipment, Email: 2633659036@qq.com; **Huan Zhang**, PhD, Associate Professor, research interests: design and theory of agricultural equipment, Email: 200501102@qau.edu.cn.
***Corresponding author: Fangyan Wang**, PhD, Professor, research interests: design and theory of agricultural equipment. College of Mechanical and Electrical Engineering, Qingdao Agricultural University, Qingdao 266109, Shandong, China. Tel: +86-15806426016, Email: wfy_66@163.com; **Xin Wang**, PhD, Lecturer, research interests: solid mechanics and its applications. College of Civil Engineering & Architecture, Qingdao Agricultural University, Qingdao 266109, Shandong, China. Tel: +86-13963958112, Email: betty_wx@126.com.

body of research results. Zhang et al.[5] utilized the DEM to establish a simulation model of cabbage, employed EDEM simulation to conduct a comparative analysis of the cutting process, and configured the designed cutting device on a self-propelled cabbage harvester for experimental validation. Shaikh et al.[6] employed the DEM to model soil-tool interactions, simulated the contact modeling between a single track and soil with different moisture contents under different water content, and compared the simulation results with the experimental results to determine the accuracy of the contact model. Makange et al.[7] utilized a discrete element method, employing a computerized testbed to investigate soil profile deformation resulting from a share plow. This approach enabled the effective prediction of the ultimate soil conditions and forces necessitated for tillage operations. Chen et al.[8] developed a coupled potato-soil separation simulation model, underpinned by the discrete element method and multi-body dynamics. Through a series of simulation tests, they identified the optimal combination of operating parameters. Field tests were then conducted to verify the model's accuracy, and the results were found to be largely consistent with those of the simulation tests. This validation process serves to substantiate the efficacy of the simulation model. Zhang et al.[4] constructed a virtual simulation model of EDEM ginger and determined the influence laws of key factors on digging resistance and soil flow. The relative error between the results of the field test and the simulation test was 7.3%, which meets the needs of farmers' use. Wang et al.[9] employed the EDEM discrete element simulation method to establish a hybrid contact model of ginger rhizome-soil, researching the impact of various digging shovels and their front blade inclination angle on digging resistance. They then proceeded to analyze the resistance changes during the ginger digging process, providing a reference for selecting the key parameters of the ginger digging shovel. Existing studies have shown that DEM simulation software can be used to more realistically simulate the interactions between soil touching parts and soil[10,11]. However, due to the limitation of EDEM software, the design optimization of agricultural machinery necessitates the consideration of material properties, motion analysis, and other factors to ensure the accuracy of the results. In certain specific instances, EDEM software can be utilized in conjunction with multi-body dynamics software.

Existing research has extensively employed the DEM-MBD coupling method to successfully simulate the interaction processes between agricultural materials and equipment such as Chinese cabbage, soil, potatoes, and ginger. This approach has effectively predicted cutting resistance, soil flow, and optimized working parameters, with simulation accuracy validated through experiments. The method has been demonstrated to have a high degree of reliability in revealing the mechanical behavior of soil-contacting components, thus providing critical references for the design of equipment. Nevertheless, the existing body of relevant simulation studies is inadequate for the purpose of harvesting operations involving multiple components and complex processes. Consequently, the expansion of the DEM-MBD coupling method's application in complex agricultural systems is imperative and necessitates novel advancements.

In light of the intricate nature of the ginger harvesting process and the substantial number of moving components, this paper employs the DEM-MBD coupling method to optimize the pertinent parameters of the device. The present study investigates the DSPGHD, with a view to analyzing the interaction relationship between ginger and soil on the one hand, and machine on the other. Furthermore, the study sets out to examine the harvesting performance of key components of ginger. The interaction model of ginger-soil-mechanism is established using DEM-MBD coupled simulation method, and the influence range and effect of key factors are determined. The Central Composite test was conducted with resistance, damage rate, and impurity rate as the response indices, and the optimal values of the key parameters of the DSPGHD were obtained. The theoretical framework encompasses the analysis of pivotal factors influencing harvesting indices, and the streamlining of the experimental scope for the design of simulation tests.

2 Materials and methods

2.1 Working principle of DSPGHD

The height of the ginger ridge is approximately 300 mm, the ridge spacing is approximately 680 mm, the mature ginger tuber is fan-shaped, and the planting agronomy is shown in Figure 1[12-14]. The trapezoidal digging shovel, the shaking and clearing device, and the clamping and conveying device are designed. The structure and working principle of the DSPGHD are shown in Figure 2. The digging device is positioned at the front of the machine and comprises a digging shovel and a hydraulic cylinder. The soil clearing device is located at the rear of the digging shovel and is connected to it via an articulated joint. It consists of a soil-clearing grill and a hydraulic motor. The clamping device is located beneath the frame and at the rear of the soil clearing device, and features a double chain design[15].

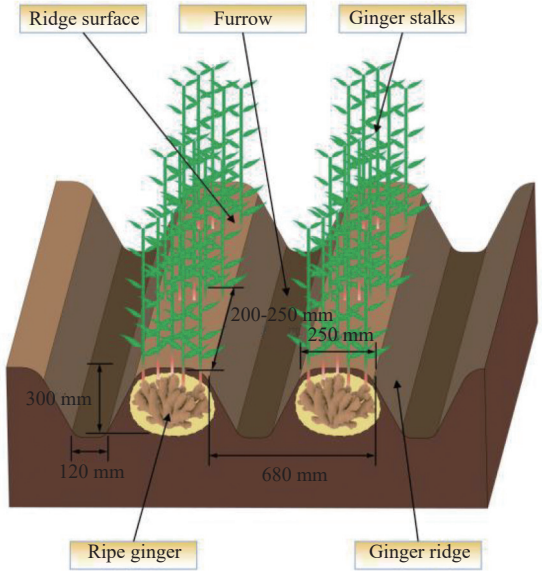

Figure 1 Ginger planting agronomy

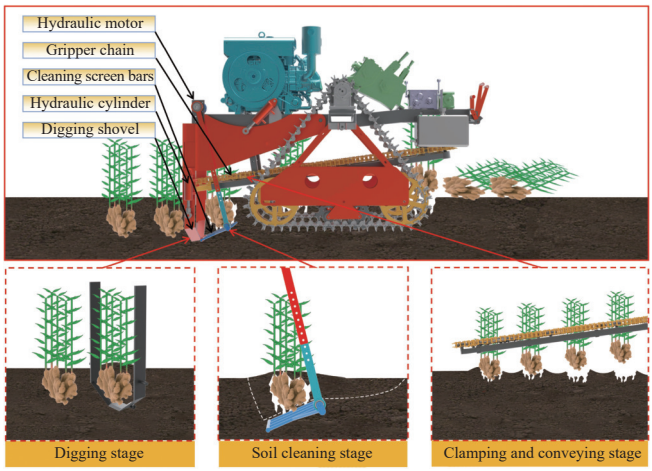

Figure 2 Structure and working principle of DSPGHD

During the harvesting operation, the soil at the root of the ginger is cut by the excavating shovel, and the ginger-soil mixture is lifted along the shovel surface to the soil clearing device. The soil is then crushed and broken by the up-and-down shaking of the shaking grill, causing the ginger and the soil to gradually separate. The ginger is separated from the soil when it reaches a certain position on the shaking bar. Subsequent to this, the ginger stalk is clamped by the clamping chain, and an angle is maintained between the clamping chain and the horizontal ground, thereby extracting the ginger from the ground and transporting it to the rear of the machine, thus completing the entire process of ginger harvesting.

2.2 Analysis of key factors affecting harvesting effectiveness

The harvesting process of ginger is a multifaceted undertaking, influenced by a multitude of factors, including the utilization of digging, soil clearing, and clamping devices, among others. In this study, the force dynamics of the ginger-soil mixture during the digging, soil clearing, and pulling processes are analyzed in conjunction with the operational principles and motion characteristics of the DSPGHD. The analysis of force is conducted separately for the three processes of digging, soil clearing, and pulling, with the objective of identifying the primary factors influencing forward resistance, damage rate, and impurity rate. This approach establishes a foundation for subsequent parameter optimization of the device.

During the process of digging, the ginger-soil mixture moves along the shovel's surface, undergoing compression and stretching. This process is influenced by various factors, including friction between the mixture and the digging shovel, adhesion forces, cutting forces, and normal loads. The adhesion and friction of the soil on the shovel surface vary due to the differing water content of different soil types. In order to analyze the source of digging resistance and reduce digging resistance, the force analysis of the ginger-soil mixture in the digging state is carried out to establish the digging mechanics model. The force analysis is shown in Figure 3[16,17].

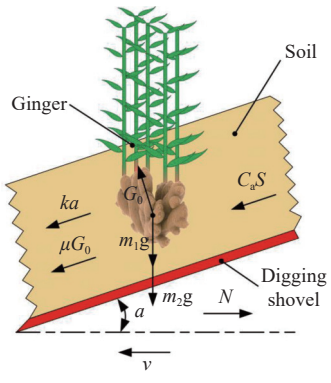

Figure 3 Force on ginger-soil mixture

The equilibrium equations of forces in the vertical and horizontal directions for the ginger-soil mixture can be obtained from Figure 3:

$$m_1g + m_2g + \mu G_0 \sin\alpha + ka\sin\alpha + C_aS\sin\alpha - G_0\cos\alpha = 0 \quad (1)$$

$$\mu G_0 \cos\alpha + ka\cos\alpha + C_aS\cos\alpha + G_0\sin\alpha - N = 0 \quad (2)$$

where, m_1 refers to the mass of ginger, kg; m_2 represents the mass of soil, kg; G_0 stands for the normal load of digging shovel, N; μ denotes the friction factor between soil and digging shovel; C_a is the adhesion force between soil and shovel; S refers to the contact area between soil and shovel, m^2; α stands for the tilt angle of the shovel surface, (°); k denotes the unit width soil cutting resistance, N; a represents the width of digging shovel, mm; N is the digging shovel forward resistance, N.

Associating Equations (1) and (2), Equation (3) is obtained as:

$$m_1g+m_2g+G_0(\mu\sin\alpha+\mu\cos\alpha-\cos\alpha+\sin\alpha)+(ka+C_aS)(\sin\alpha+\cos\alpha)-N=0 \quad (3)$$

An analysis was conducted to ascertain the factors influencing the ginger-soil mixture during the digging process. It was deduced that the factors in question included μ, C_a, and α. Based on empirical evidence, it was determined that the tilt angle α of the digging shovel surface was 10°, and the digging depth was ≤ 250 mm. Once the harvester and the harvesting environment were stabilized, μ, C_a, and α tended to be stabilized.

In the process of soil clearing, the ginger-soil mixture is continuously lifted and dropped under the action of the up and down beat of the shaking bar, and the soil is broken and separated from the ginger. This link is pivotal to the ginger harvesting process, with the FS and LCB of the shaking bar directly impacting the damage rate and soil content of the ginger. Consequently, the force on the ginger-soil mixture during the soil clearing process was analyzed[18,19]. The configuration of the soil clearing device is depicted in Figure 4. The crank (AB) is driven by the hydraulic motor to rotate. (BC) is the connecting rod, (CD) is the rocker, the rocker is connected to the soil clearing bar, and (AD) is the frame. The rotation of the hydraulic motor drives the rocker (CD), which in turn moves the soil-clearing bar up and down, thereby facilitating the shaking process.

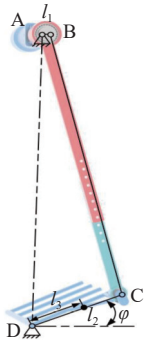

Figure 4 Structure of the soil clearing device

The angular velocity at point C is shown in Equation (4):

$$\omega_D = \frac{l_1\omega\cos\omega t}{l_2} \quad (4)$$

where, ω_D stands for the rocker angular velocity, rad/s; l_1 refers to the crank length, m; l_2 represents the rocker length, m; ω denotes the crank angular velocity, rad/s; t represents the time, s.

The velocity and acceleration at any position on the rocker satisfy Equations (5) and (6):

$$v' = \frac{l_1\omega\cos\omega t}{l_2}\cdot l_3 \quad (5)$$

$$a' = \frac{dv_C}{dt} = -\left(\frac{l_1l_3}{l_2}\right)\omega^2\sin\omega t \quad (6)$$

where, v' refers to the velocity at any position on the rocker, m/s; l_3 stands for the distance from any position on the rocker to point D, m; a' denotes the acceleration at any position on the rocker, m/s^2.

During the process, the shaking bar provides a reaction force to the ginger-soil mixture, causing it to rebound and oscillate. The process is analyzed in terms of momentum to obtain the momentum

Equation (7)[18]:

$$(m_1+m_2)(v-v_0)=\int_{t_1}^{t_2}F\mathrm{d}t \tag{7}$$

where, m_1 is the mass of ginger, kg; m_2 stands for the mass of soil, kg; v refers to the velocity of the ginger-soil mixture leaving the clearing bar at the instant, m/s; v_0 stands for the velocity of the ginger-soil mixture touching the clearing bar, m/s; F denotes the combined force of the ginger-soil mixture by the clearing bar, N.

As the soil-clearing process progresses, the soil mass enveloping the ginger gradually diminishes. The soil mass correction factor, designated Z, is introduced to derive Equation (8):

$$m_2=m_2'l_3Z \tag{8}$$

where, m_2' refers to the mass of the soil when the ginger-soil mixture first comes into contact with the clearing bar, kg; Z stands for the soil mass correction factor.

In view of the fact that the period of contact between the ginger-soil mixture and the soil-clearing bar is very brief, it is hypothesized that the change of φ is linear; accordingly, Equations (6) to (8) are utilized to obtain the support force of the ginger-soil mixture on the soil-clearing bar, as shown in Equation (9):

$$F_N=\left(m_1+m_2'l_3Z\right)g\int_{\varphi_1}^{\varphi_2}\cos\varphi\mathrm{d}\varphi-\left(m_1+m_2'l_3Z\right)\left(\frac{l_1l_3}{l_2}\right)\omega^2\sin\omega t \tag{9}$$

where, F_N refers to the support force of ginger-soil mixture on the soil-clearing bar, N; φ stands for the angle between the clearing bar and the horizontal plane, (°); φ_1 denotes the angle of inclination of the bar when the ginger-soil mixture and the soil-clearing bar are just in contact, (°); φ_2 is the angle of inclination of the bar when the ginger-soil mixture is just separated from the soil-clearing bar, (°).

The analysis demonstrates that the ginger-soil mixture is influenced by factors such as ω_D, l_2, and φ, which are present during the soil clearing process. The digging shovel primarily functions as a cutting tool, with the objective of loosening the soil and separating the root soil from the ginger. Consequently, the primary focus of this analysis is to examine the impact of the soil clearing process on the ginger-soil mixture. The rocker angular velocity ω_D has been found to be directly proportional to its FS f. Consequently, the FS f is a central focus in the experimental design.

At the moment of clamping and lifting, the clamping chain makes contact with the ginger stalks, causing them to tilt at an angle. At this point, the ginger-soil mixture is subjected to the clamping and lifting force, its own gravity, and the adhesion force provided by the soil. The forces on the ginger-soil mixture during the clamping process are shown in Figure 5[20-22].

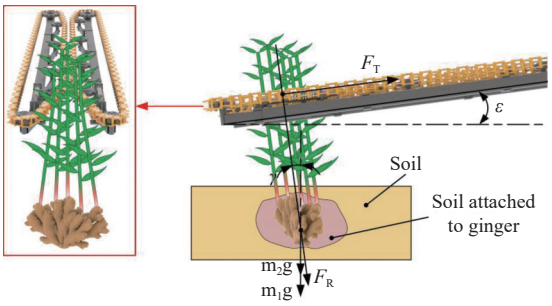

Figure 5 Schematic representation of the force on the ginger-soil mixture at the moment of clamping and lifting

Equation (10) needs to be satisfied to ensure that ginger is lifted away from the soil at the moment of clamping and lifting:

$$F_T\sin\varepsilon\geq\left(m_1+m_2'l_3Z\right)g+F_R\cos\gamma \tag{10}$$

where, F_T refers to the clamping chain pulling force, N; ε stands for the angle between the clamping chain and the horizontal plane, °; F_R denotes the soil adhesion force on the ginger-soil mixture, N; γ is the ginger stalk inclination angle, °.

It is analyzed that the ginger-soil mixture is affected by ε and F_R during the clamping and lifting process. ε is controlled at about 8°, which is too large to lead to too high a fuselage height, and too small to lead to too long a fuselage length. F_R is affected by the clearing process, so it is analyzed and researched with emphasis on the clearing process.

In summary, the present study investigates the effect of a harvesting device for ginger on a ginger-soil mixture. The device in question involves a digging, shaking, and pulling mechanism. The analysis focuses on the effect of the IACB φ, the LCB l_2, and the FS f on the harvesting effect.

2.3 Modeling of EDEM-RecurDyn coupling

2.3.1 Discrete element modeling

The soil type of ginger cultivation in the Shandong province area is predominantly loamy. In order to accurately simulate the soil-crop-mechanism interactions characteristics and to ensure the realism and efficiency of the simulation analysis, the Hertz-Mindlin with Bonding model was utilized as the mechanical contact model between soil particles. The model of the ginger plant was established in SolidWorks and imported into the EDEM soil tank[23,24], which has dimensions of 4000×1360×580 mm. The particle factory was established and the particles were filled statically and quickly to form the ginger ridges by settling, stacking, and generating bond action. The radius of the soil particles was set to 6 mm, the soil density to 1.56×10³ kg/m³, Poisson's ratio to 0.4, and the shear modulus to 1×10⁶ Pa. As indicated in Table 1, the soil model contact parameters were obtained through a combination of previous simulation model calibration work and reference to the relevant literature[25-27]. The ginger model is depicted in Figure 6.

Table 1 Contact parameters for soil modeling

Item	Parameter	Value
Hertz-Mindlin with Bonding	Normal Stiffness per unit area/N·m^{-3}	2.85×10^7
	Shear Stiffness per unit area/N·m^{-3}	1.3×10^7
	Normal Strength/Pa	5.3×10^4
	Shear Strength/Pa	7×10^3
	Bonded Disk Scale	1.1
Soil parameters	Density/kg·m^{-3}	1.56×10^3
	Poisson's ratio	0.4
	Shear modulus/Pa	1×10^6
	Physical radius/mm	6
	Soil-soil Coefficient of Restitution	0.2
	Soil-soil Coefficient of Rolling Friction	0.3
	Soil-soil Coefficient of Static Friction	0.4
Ginger parameters	Density/kg·m^{-3}	1.16×10^3
	Poisson's ratio	0.28
	Shear modulus/Pa	1.21×10^6
	Ginger-soil Coefficient of Restitution	0.4
	Ginger-soil Coefficient of Rolling Friction	0.03
	Ginger-soil Coefficient of Static Friction	0.56

2.3.2 Multi body dynamics model

A 3D model of the DSPGHD was constructed in SolidWorks (as illustrated in Figure 7). Subsequent to the assembly stage, the 3D model was saved in STEP format and imported into the RecurDyn pre-processing interface[28,29]. The model attributes were

set to correspond to the parameter settings in EDEM, the coordinate system was aligned with the EDEM coordinate system, the excavation depth was set to 250 mm, the forward speed of the device was set to 0.25 m/s, the up-and-down oscillating motion of the clearing bar around the slewing center was added, and the conveying motion of the clamping chain was added subsequently.

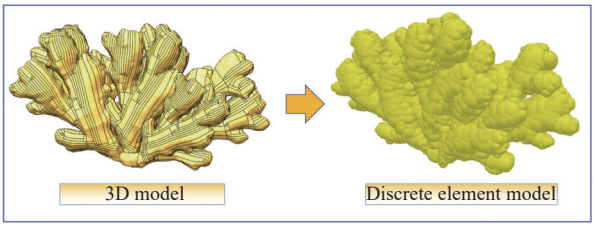

Figure 6 The ginger model

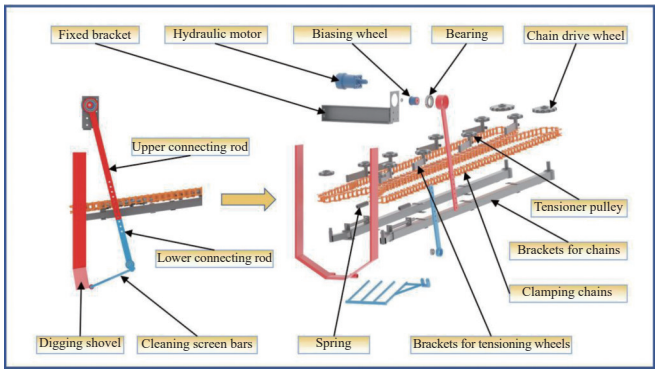

Figure 7 3D model of the DSPGHD

2.3.3 Coupled simulation model

The External SPI coupling interface was opened in RecurDyn, and the DSPGHD was exported as a wall file and imported into the EDEM software[30]. The material properties and contact parameters of the imported wall file were then added in EDEM software, with 65Mn selected as the material for the soil-touching parts, having a density of 7.85×10^3 kg/m^3, a Poisson's ratio of 0.35, and a shear modulus of 7.9×10^{10} Pa. The specific parameters are shown in Table 2. The time step is 7×10^{-5} s and the data is saved every 0.1 s. In the RecurDyn simulation, the time step is equivalent to that employed in EDEM, with the simulation calculation being conducted. In accordance with the preceding related literature, the simulation time is set to 8 s[31], and the ginger within 2 m can be harvested, which is approximately 10 plants. This can be considered a reflection of the actual harvesting operation. When the DSPGHD harvests the ginger in the soil, RecurDyn and EDEM interact with the kinetic and discrete element information in both directions, and the principle of the coupled simulation process of DEM-MBD is demonstrated in Figure 8[32].

Table 2 Material and contact parameters of the DSPGHD

Parameter	Value
65Mn density/(kg·m^{-3})	7.85×10^3
65Mn Poisson's ratio	0.35
65Mn shear modulus/Pa	7.9×10^{10}
65Mn-soil Coefficient of Restitution	0.3
65Mn-soil Coefficient of Rolling Friction	0.05
65Mn-soil Coefficient of Static Friction	0.4

2.3.4 Single factor simulation test design

In order to explore the range of main factors affecting the operation quality of the DSPGHD, a single-factor simulation test was carried out. The IACB φ, the LCB l_2, and the FS f were selected as the test factors. The resistance of the device to advancement, the force on the ginger, and the flow of the soil were measured and analyzed. The intermediate level of the single-factor test was set as follows: the IACB was set at 7°, the FS was set at 5 Hz, and the LCB was set at 280 mm. The data of each test index were exported from the EDEM post-processing interface, and the image was drawn using Origin2024 for analysis and exported as a cloud map of soil flow rate. The process of the ginger harvest simulation test is illustrated in Figure 9[8].

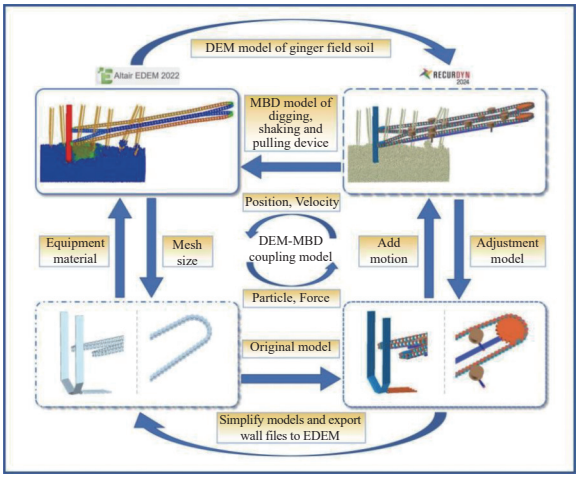

Figure 8 Principle of coupled DEM-MBD simulation

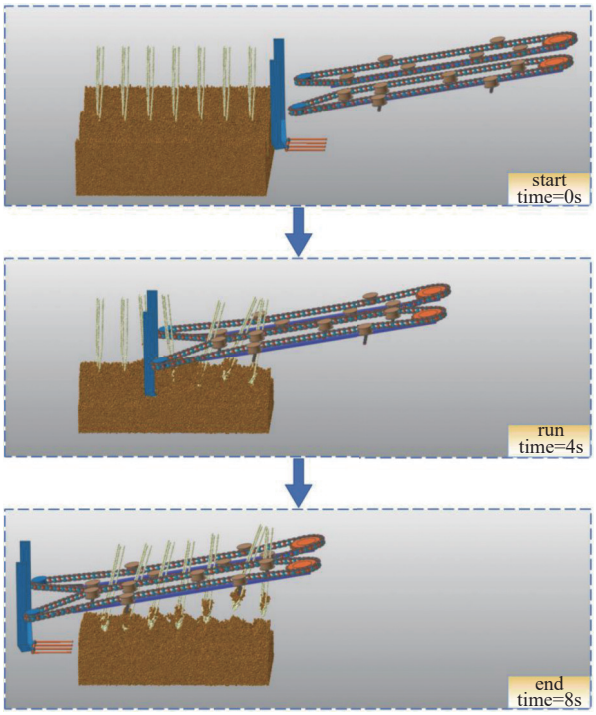

Figure 9 Simulation test process for ginger harvesting

2.4 Field tests

2.4.1 Test conditions

A field test was conducted on 23 October 2024 at the ginger planting base in Shibu Town, Changyi, Weifang, Shandong Province (as shown in Figure 10). The primary objective of the test was to ascertain the optimal design parameters for the DSPGHD in the machine[31]. The test variety was Changyi cotton-ginger, with a total height of 900-1000 mm for the ginger plant, 180-200 mm for the sub-ginger, a soil moisture content of 12.56%, and the soil

compactness was 1.7 MPa. The power source for the entire apparatus was a 13.2 kW Changchai single-cylinder diesel engine, and the digging resistance and the FS were determined by means of a pulling pressure sensor and a rotary encoder respectively.

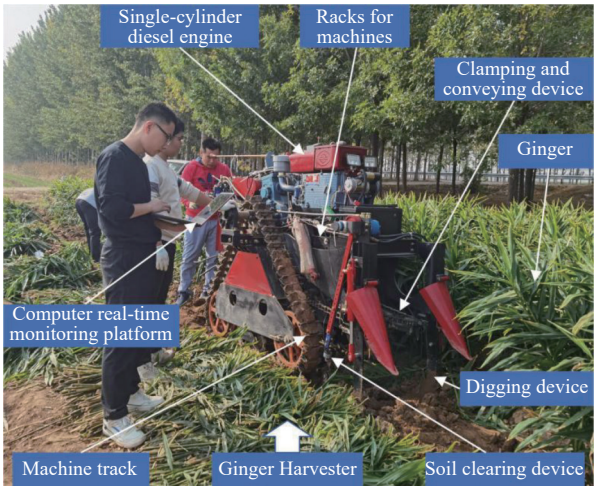

Figure 10 Field tests

2.4.2 Evaluation indicators

As there exists no specific standard for ginger harvesting in China, the relevant indices were evaluated in accordance with the standard of the Self-propelled Onion Harvester (T/NJ 1110-2018). Each group of test machines was operated for a distance of 20 m, after which the digging resistance, impurity content, and damage rate were determined[33]. The digging resistance was directly read from the data acquisition system, while the impurity content and damage rate were calculated according to the formula.

1) Resistance

At the conclusion of the test, the forward resistance of each stage of the test area was derived directly from the cloud platform of the data acquisition system and averaged.

2) Impurity rate

Ginger in the test area was collected in order to ascertain its total mass. A second determination was made after the soil adhering to the ginger had been removed, and the impurity rate was calculated using the following formula:

$$B = \frac{Q - Q_1}{Q} \times 100\% \quad (11)$$

where, B refers to the impurity rate of ginger in the test area; Q represents the total mass of ginger in the test area; Q_1 stands for the total mass of ginger in the test area after removing soil and impurities.

3) Damage rate

The damage rate is calculated based on the total mass in the test area and the mass of the damaged fracture:

$$P = \frac{M}{Q} \times 100\% \quad (12)$$

where, P refers to the damage rate of ginger in the test area; M denotes the total mass of damaged ginger in the test area.

2.4.3 Test scheme

In accordance with the single-factor simulation test, the IACB X_1, the FS X_2, and the LCB X_3 were selected as the test factors, and the forward resistance Y_1, the damage rate Y_2, and the impurity rate Y_3 were selected as the test indices. It was found that if the IACB was too large or too small, the resultant clearing effect was negligible, and it was impossible to lift the ginger to the exposed soil surface. Furthermore, if the FS was too fast, the ginger was seriously damaged. It is also impossible to ensure the damage rate. If the FS is too slow, the forward resistance of the machine will increase and the clearing effect will not be obvious. The LCB also plays an important role in the forward resistance of the machine and the rate of soil removal. If the length is too long, the forward resistance increases, leading to an increase in the power consumption of the whole machine. If the length is too short, the effect of soil clearing is not significant.

The parameter adjustment process of each factor is as follows: control the IACB by adjusting the length of the connecting rod, adjust the rotation speed of the hydraulic motor to adjust the frequency of the clearing bar shaking by adjusting the speed of the hydraulic motor in the PLC control interface, and change the LCB by replacing the clearing bar with different lengths. When the machine is harvesting in the field, it is put into the second gear, and the forward speed is controlled at about 0.25 m/s.

In summary, the Central Composite method, as implemented in Design-Expert software, was utilized to devise a three-factor, five-level orthogonal experimental design. The test factors encompassed the IACB (X_1), the FS (X_2), and the LCB (X_3). The coding table of test factors is shown in Table 3[34,35].

Table 3 Test factor codes

Code	Test factors		
	IACB	FS	LCB
1.682	19	6	294
1	15	5	280
0	9	4	260
–1	3	3	240
–1.682	–1	2	226

3 Results

3.1 Interaction between device and harvesting effect based on DEM-MBD coupling

3.1.1 Influence of different factors on forward resistance

Looking closely at Figure 11a, it can be clearly seen that when the IACB are set at the two levels of –1° and 3°, their effects on the forward resistance of the machines do not show a significant difference. In particular, the magnitude of the mean forward resistance at these two angles is almost the same, which means that these two angles have a comparable effect on resistance in terms of average effect. However, it is worth noting that the degree of dispersion of the forward resistance is relatively large at an initial angle of –1° for the bars, which reflects a wider range of fluctuations in resistance. This situation is obviously unfavorable to the stable harvesting of the machine, as the large resistance fluctuation may lead to the unstable operation of the machine, which in turn affects the harvesting efficiency and the quality of operation. On the other hand, when the initial angle was varied in the range of 3°-15°, the difference in the effect of each test level on the forward resistance became more obvious. This finding suggests that in order to further optimize the performance of machinery, more detailed testing and optimization work can be considered in this angle range.

Analyzing Figure 11b, it can be clearly seen that when the bar FS is set in the interval of 3-7 Hz, its effect on the forward resistance shows a more obvious difference. This means that in this frequency range, the FS has a more direct and obvious effect on the resistance experienced by the machine. By contrast, when the FS

was set at 1 Hz or 9 Hz, its effect on the forward resistance was relatively weak and the difference was not significant. This finding provides a valuable reference for the subsequent adjustment of the FS in order to optimize the performance of the machine.

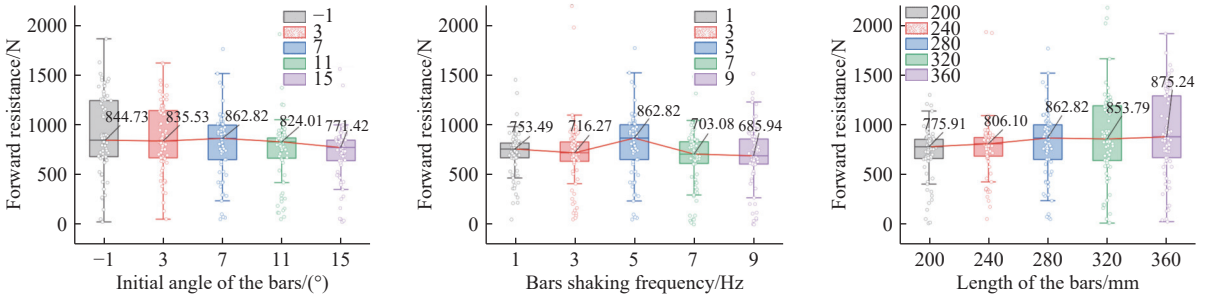

a. Influence of IACB on the forward resistance b. Influence of FS on forward resistance c. Influence of LCB on forward resistance

Figure 11 Influences of different factors on forward resistance

As shown in Figure 11c, the effect of these two lengths on the forward resistance does not show a significant difference when the LCB are 320 mm and 360 mm, respectively. More critically, the degree of dispersion of the forward resistance is relatively large in both length conditions, indicating that the magnitude of the resistance is not stable enough and there is a certain degree of volatility. This situation is also not conducive to the stable harvesting operation of the machine. Therefore, it is necessary to further explore a more appropriate size range in the selection of LCB to ensure that the machine can show more stable and efficient performance in actual operation.

3.1.2 Influences of different factors on forces on ginger

The analysis of Figure 12a indicates that the different settings of the IACB did not have a significant effect on the force applied to the ginger. Specifically, the force applied to the ginger did not show significant variations at the various angle levels tested. This finding suggests that adjusting the IACB may not be a key factor in optimizing the force on the ginger under the current test conditions. Consequently, in subsequent machine design, the emphasis can be directed towards the optimization of other parameters, without the necessity of excessive preoccupation with the IACB.

As demonstrated in Figure 12b, the FS has a significant impact on the force exerted on the ginger. The force on the ginger increased significantly when the FS was 7 Hz and 9 Hz, even reaching a peak value of 100 N at some specific moments. This level of force is close to or exceeds the limit of the ginger's ability to withstand and is therefore likely to result in breakage of the ginger during the harvesting process, affecting the final quality and efficiency of the harvest. On the contrary, when the FS was between 1-5 Hz, the force on the ginger was relatively stable and the difference in the effect on the force on the ginger between the different frequency levels was not obvious. This finding provides a clear direction for optimization, namely to refine the FS settings in the range of 1-5 Hz in subsequent experiments. The objective is to identify the optimal FS parameter that will ensure the force applied to the ginger is as low and stable as possible during the harvesting process.

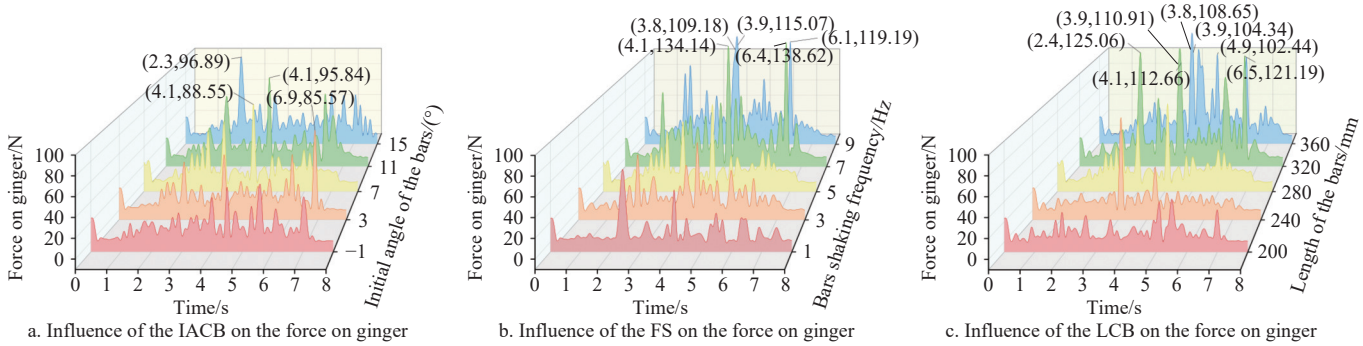

a. Influence of the IACB on the force on ginger b. Influence of the FS on the force on ginger c. Influence of the LCB on the force on ginger

Figure 12 Influence of factors on forces on ginger

Analysis of Figure 12c demonstrates a substantial impact of varying the LCB on the force exerted on the ginger. When the LCB was set between 200 and 280 mm, the force on the ginger exhibited enhanced stability and diminished fluctuation range. This indicates that within this length range, the bars can effectively regulate the force on the ginger during the harvesting process, thereby mitigating the risk of breakage. However, when the LCB was increased to 320 mm and 360 mm, the maximum force on the ginger increased significantly and the fluctuation became abnormally pronounced. This unstable force situation is very likely to lead to ginger damage and breakage of the ginger during harvesting, thus affecting the quality and efficiency of the process. Consequently, in the subsequent optimized design of the machine, further investigation is required into the optimum setting of the LCB in the range of 200-280 mm in order to minimize the breakage rate of the ginger while maintaining the efficient operation of the machine.

3.1.3 Influences of different factors on the effectiveness of soil loosening and breakage

Plot a graph of soil flow rate at a given time for each group of tests and discuss and analyze the effect of each factor on the effect of soil loosening and breakage[36].

Observing the effect of the IACB on the soil flow rate shown in Figure 13a, it can be seen that when the IACB was at –1° and 3°, the change in soil flow rate was not significant, indicating that the loosening effect of the bars on the soil was relatively weak and the soil flow rate was kept stable in this angular interval. Similarly, when the IACB was 11° and 15°, the difference in soil flow rate

was not significant, indicating that adjusting the angle of the bars had a limited effect on the soil flow rate in this interval. However, it is worth noting that when the IACB was increased from 3° to 11°, the soil flow velocity showed a significant upward trend, a finding that provides an important clue for subsequent experimental optimization, which is that fine-tuning within this angle range may be helpful in achieving more efficient soil loosening and breaking effects while avoiding unnecessary damage to the ginger.

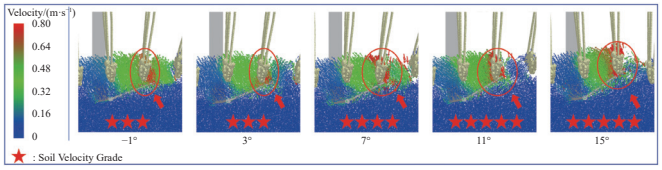

a. Influence of IACB on effectiveness of soil loosening and breakage

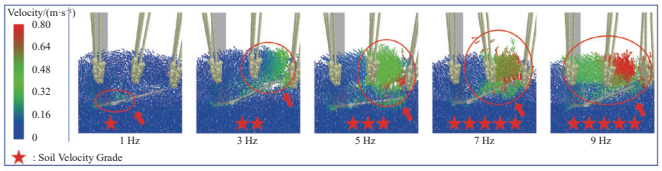

b. Influence of FS on effectiveness of soil loosening and breakage

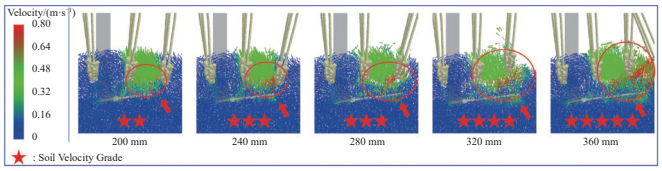

c. Influence of the LCB on effectiveness of soil loosening and breakage

Figure 13 Influences of different factors on effectiveness of soil loosening and breakage

The effect of FS on soil flow velocity in Figure 13b shows that soil flow velocity increases significantly with increasing FS. This trend suggests that increasing the FS can promote soil loosening and flow more effectively. However, when the FS reached 7 Hz and 9 Hz, the phenomenon of soil splashing occurred, which not only means that the soil loosening effect is too strong, but also may cause physical damage to the ginger, such as breakage or scratches, which may affect the quality and yield of ginger. Therefore, in order to achieve efficient soil loosening, the FS of the bars must be properly controlled to avoid unnecessary damage to the crop.

Observation of the effect of the LCB on the area of soil disturbance in Figure 13c showed that although a slight disturbance of the soil could be achieved at the LCB of 200 mm, the area of disturbance was relatively small and might not be sufficient to loosen the soil completely. Conversely, when the LCB was increased to 320 mm and 360 mm, the soil disturbance range was significantly increased, which helped to loosen the soil more deeply, but also led to the tilting phenomenon of the ginger plant, which not only increased the instability of the ginger harvesting process, but also may cause difficulties in the subsequent pulling operation and reduce the harvesting efficiency. Therefore, choosing the right LCB to find the best balance between soil loosening effect and ginger growth stability is the key to optimizing the harvesting equipment.

In order to further analyze the effect of the DSPGHD on soil loosening and breaking, the curves of soil kinetic energy at the level of each factor are introduced here[28]. From Figure 14a, it can be seen that the difference in the IACB on the kinetic energy of the soil is not significant and can be ignored when analyzing the effect of the key factors on the kinetic energy of the soil. As illustrated in Figure 14b, the variation in the change in soil kinetic energy is not substantial when the FS is between 5 and 9 Hz. However, the kinetic energy of the soil is considerably less at 1 Hz and 3 Hz than at the remaining three levels, particularly at 1 Hz. At this frequency, the change in soil kinetic energy is negligible, and the total kinetic energy provided by the FS to the soil is 15.05 J. According to Figure 14c, the maximum kinetic energy imparted to the soil is observed at the LCB of 360 mm, with a value of 175.74 J. As the LCB is reduced, the kinetic energy of the soil at the remaining four levels diminishes. This observation indicates that an increase in both the FS and the LCB results in more soil particles being contacted within a given time interval. Consequently, the bar performs a greater amount of work on the soil, leading to an increase in the soil's kinetic energy. This, in turn, leads to the soil being loosened and broken down effectively.

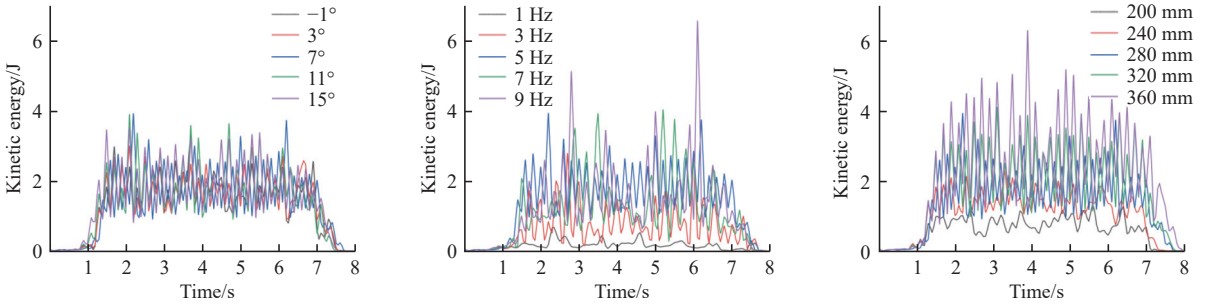

a. Influence of IACB on kinetic energy of soil b. Influence of FS on kinetic energy of soil c. Influence of LCB on kinetic energy of soil

Figure 14 Influences of different factors on the kinetic energy of the soil

In summary, the present study combined the DEM-MBD single factor simulation test and the agronomic requirements of ginger harvesting with the machine's matching dimensions, thereby determining the IACB φ (3°-15°), the FS f (3-5 Hz), and the LCB l_2 (240-280 mm) to be selected as the test factors, and designing a three-factor five-level orthogonal test to provide theoretical support and foundation for the optimization of the parameters of the DSPGHD in the future.

3.2 Results and analyses of field tests

3.2.1 Results of field tests

The test design and analysis were conducted using Central Composite of Design-Expert 13 software, and the test results are presented in Table 4.

3.2.2 Analysis of variance (ANOVA) for field tests

The test results were analyzed by analysis of variance (ANOVA), and multiple regression was fitted to the test data using Design-Expert 13 software. This resulted in the regression equations for forward resistance Y_1, damage rate Y_2, and impurity rate Y_3[37].

1) Regression modeling and significance testing of forward resistance

The analysis demonstrates that the model exhibits an extremely significant fit (p<0.01) and a misfit term of p=0.1583. This indicates

Table 4 Test scheme and results

Serial number	Test factors			Y_1/N	Y_2/%	Y_3/%
	X_1/(°)	X_2/Hz	X_3/mm			
1	19	4	260	2462	5.15	5.92
2	9	4	260	1585	4.47	3.79
3	3	3	280	2186	6.38	9.21
4	15	5	240	1840	7.18	4.74
5	9	4	260	1606	4.32	4.35
6	9	4	260	1697	4.1	3.91
7	15	5	280	2391	6.36	4.21
8	9	4	294	2413	6.93	7.62
9	9	4	226	1472	7.24	7.93
10	9	4	260	1664	4.56	4.38
11	15	3	280	2395	6.95	9.14
12	3	3	240	2098	5.62	9.68
13	9	6	260	1337	6.75	3.79
14	9	4	260	1517	5.02	3.74
15	–1	4	260	2249	5.32	6.15
16	15	3	240	2076	5.53	9.32
17	3	5	280	2192	6.55	6.25
18	9	4	260	1497	3.93	4.15
19	3	5	240	1607	6.89	5.97
20	9	2	260	1871	5.28	11.06

that no other major factors are affecting the indicators. Among them, the regression terms X_2, X_3, X_1^2, X_3^2 are extremely significant (p<0.01), X_1, X_2X_3 are significant (p<0.05), while the rest of the terms are not significant (p≥0.05). Excluding the insignificant regression terms, the regression Equation is obtained as:

$$Y_1 = 1597.12 + 71.85X_1 - 112.06X_2 + 228.06X_3 + 91.12X_2X_3 + 297.64X_1^2 + 142.26X_3^2 \quad (13)$$

The regression coefficient test of Equation (13) provides an indication of the magnitude of the effect of each factor on the forward resistance, as follows: LCB > FS > IACB.

2) Regression modeling and significance testing of damage rate

The analysis revealed that the fit of the model is extremely significant (p<0.01), and it also revealed the misfit term p=0.3904. The misfit term was found to be non-significant, indicating that no other major factors are affecting the indicator. Among them, the regression terms X_2, X_1^2, X_2^2, X_3^2 were found to be extremely significant (p<0.01), X_2X_3 was found to be significant (p<0.05), while the rest of the terms were found to be insignificant (p≥0.05), and the regression Equation was obtained by eliminating the insignificant regression terms as:

$$Y_2 = 4.41 + 0.34X_2 - 0.4175X_2X_3 + 0.3888X_1^2 + 0.4455X_2^2 + 1.01X_3^2 \quad (14)$$

The regression coefficient test of Equation (14) provides a quantitative indication of the effect of each factor on the damage rate, as illustrated below: FS > LCB > IACB.

3) Regression modeling and significance testing of impurity rate

The analysis demonstrates that the model exhibits an extremely significant (p<0.01) fit and a non-significant misfit term (p= 0.0889). This finding indicates that no other major factors are affecting the indicator. Among them, the regression terms X_2, X_1^2, X_2^2, X_3^2 are extremely significant (p<0.01), X_1, X_1X_2 are significant (p<0.05), while the rest of the terms are not significant (p≥0.05). Excluding the insignificant regression terms, the regression Equation is obtained as:

$$Y_3 = 4.06 - 0.3012X_1 - 1.92X_2 - 0.3550X_1X_2 + 0.8057X_1^2 + 0.8866X_2^2 + 1.37X_3^2 \quad (15)$$

The regression coefficient test of Equation (15) provides a quantitative indication of the effect of each factor on the impurity rate, as illustrated below: FS > IACB > LCB.

According to the findings of the regression analysis, the IACB, the FS, and the LCB were adjusted to the zero level, and the significant interaction response surface was plotted to analyze the influence of the test factors on the forward resistance, damage rate, and impurity rate. The response surface is shown in Figure 15.

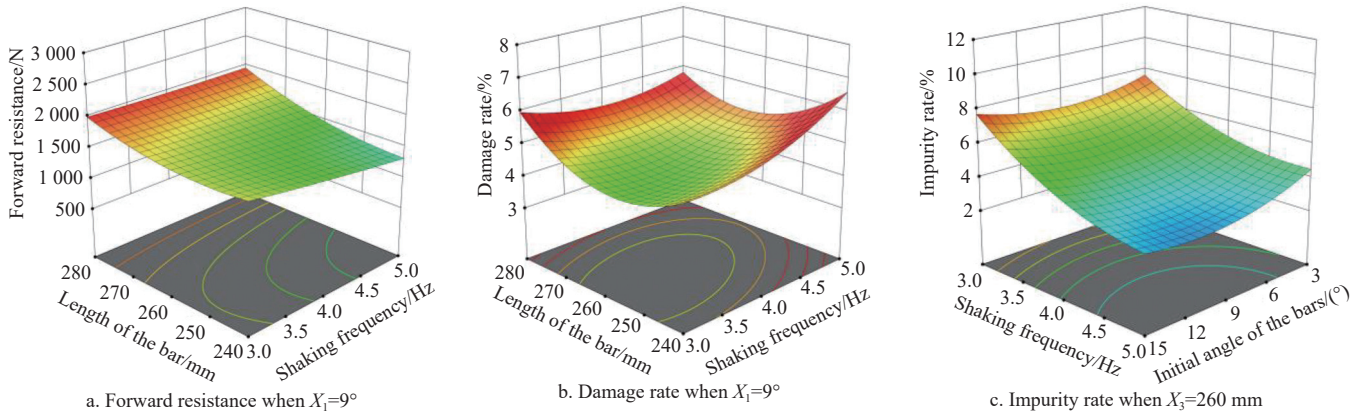

a. Forward resistance when X_1=9° b. Damage rate when X_1=9° c. Impurity rate when X_3=260 mm

Figure 15 Response surfaces for the effect of interactions on test metrics

3.2.3 Relationship between factors and indicators

As demonstrated in Figure 15a, when the IACB is set at 9°, with the LCB constant, the forward resistance exhibits a tendency to decrease with an increase in the FS. For an identical IACB, a decrease in FS results in a deterioration in soil disturbance, leading to a reduction in soil loosening and crushing effectiveness. This, in turn, results in an increase in forward resistance. In the case of a specific FS, the forward resistance increases with an increase in the LCB. In the same bar initial angle and FS, the longer the LCB, the larger the amount of soil that is instantly contacted by the bar. Conversely, the effect of soil loosening is more pronounced at shorter LCB, resulting in a smaller amount of soil being instantly contacted.

As illustrated in Figure 15b, when the LCB is constant and the IACB is set at 9°, the damage rate displays a parabolic trend, initially decreasing and subsequently increasing with higher FS. At

constant IACB, elevated dithering frequencies intensified the mechanical slaps exerted on ginger rhizomes, consequently elevating the damage rate. Conversely, lower FS resulted in suboptimal soil disturbance, leading to reduced soil fragmentation efficiency and increased resistance. This phenomenon amplified the interaction forces between ginger and soil, thereby increasing the damage rate. Under constant FS conditions, the damage rate demonstrated a parabolic relationship with the LCB, characterized by an initial decrease followed by an increase. At identical IACB and FS, longer bars simultaneously engaged more ginger plants, exacerbating mutual compression and consequently increasing damage rates. Conversely, shorter bars demonstrated inferior lifting efficiency, resulting in greater pulling resistance and correspondingly higher damage rates during the harvesting process.

As demonstrated in Figure 15c, when the LCB was fixed at 260 mm and the FS was constant, the impurity rate exhibited a tendency to decrease, followed by an increase, with an increase in the IACB. For a given LCB, an increase in the IACB resulted in a worsening of the loosening effect on the ginger-soil mixture, leading to an elevated impurity rate. Conversely, when the IACB was fixed, the impurity rate exhibited a decline with an increase in the FS. At a constant bar length and initial angle, a reduction in FS resulted in a diminished effect of the bars on the disturbance and loosening of the ginger-soil mixture. Consequently, soil and other debris adhered to the surface of the ginger, leading to an elevated impurity rate.

3.2.4 Optimization of the objective function and results

In order to ascertain the optimal operating parameters of the digging and clearing device and optimize its working parameters, the three regression models were solved by using the optimization module in Design-Expert 13 software. The linear programming mathematical model was employed to optimize the three parameters in the objective function, taking the minimum forward resistance Y_1, the minimum damage rate Y_2, and the minimum impurity rate Y_3 as the objectives. This approach yielded optimal parameter combinations, and the optimization results are as follows: the IACB is 8.7°, the FS is 4.24 Hz, and the LCB is 256 mm. Under these conditions, the device operates optimally, with a forward resistance of 1526 N, a damage rate of 4.57%, and an impurity rate of 3.74%.

4 Discussion

The interaction between machinery and soil and crop is widely regarded as the crop damage rate and resistance of the device. The method to reduce the damage rate and resistance is generally to change the geometry and structure of key components, and to use mechanical design and dynamics analysis for research[38-40]. In recent years, the use of EDEM software to simulate and analyze the harvesting process, simulating the resistance and other key indicators of machinery in the field test, has become the mainstream in machinery design[4]. In this paper, the calibration of the relevant parameters of the discrete element model is still to be improved. The size of the granular body was increased to enhance computational speed; however, this also resulted in a reduction in model accuracy. Consequently, it is imperative that the calibration of the granular body is conducted using a computer with superior computational capabilities. Furthermore, ginger is cultivated in a variety of soil environments; however, the current study focuses exclusively on the sandy loam soil modeling. The model is a single type; if the conditions permit, it can be adapted to model different types of soil.

The application of coupled DEM-MBD simulation to model the interaction of machinery with soil and crop is an emerging field[31], yet the depth of related research is limited. In this paper, we analyzed the effects of the IACB, the LCB, and the FS on the forward resistance, the force of ginger, and the effect of soil loosening in the ginger harvesting device by the DEM-MBD coupling method. It is a novelty that the factor influence interval was obtained. The coupled simulation model of EDEM and RecurDyn software adopted in this paper has been shown to simulate the operation process and results of a ginger harvesting device with a high degree of accuracy. The method enables precise optimization of the design parameters of the core components of the ginger harvesting device and the visualization of the operation effect statistics. In future research on ginger harvesting equipment, the DEM-MBD coupled simulation analysis will receive greater attention and application.

As the harvesting of various target crops and different soil conditions by ginger harvesting devices poses the most significant challenge at present, the proposed digging-shaking-pulling ginger harvesting method can also be applied to other varieties and soil conditions. In the future, research will be conducted on the adaptability and stability of ginger harvesting devices for different regions and varieties of ginger.

5 Conclusions

This paper presents a novel device for harvesting ginger, known as the digging-shaking-pulling type. This device is designed to address the challenges posed by high digging resistance, impurity rate, and breakage rate during the harvesting process. Through a theoretical analysis of the interactions between the ginger, soil, and mechanisms in the three working processes of digging, shaking, and pulling, the study identifies the key influencing factors that determine the harvesting efficacy. These factors include the IACB φ, the LCB l_2, and the FS f. The key factors obtained from the theoretical analysis were analyzed by single-factor simulation, and a coupled DEM-MBD simulation model was established to study the influence law and effect of the key factors on the test indices through the simulation test and post-processing. The range of values of the factors was determined, which provided a theoretical basis for the field test. A three-factor five-level orthogonal test (Central Composite) was designed using Design-Expert software for field tests, and the response surface and multi-objective function optimization were used to obtain a better combination of key factors affecting the harvesting indices. The IACB was 8.7°, the LCB was 256 mm, and the FS was 4.24 Hz. At this time, the sizes of the various harvesting indices were as follows: the forward resistance was 1526 N, the damage rate was 4.57%, and the impurity rate was 3.74%. This determines the key component parameter combinations under the better harvesting conditions, and the parameter combinations satisfy the requirements of the farmers and promote the development of China's ginger mechanized harvesting industry.

Acknowledgements

This study was supported by the Taishan Scholar Youth Expert Project (Grant No. tsqn202306243), the National Natural Science Foundation of China (Grant No. 52275258), and the Qingdao Science and Technology Benefiting the People Demonstration and Guidance Special Program (22-3-7-xdny-14-nsh).

[References]

[1] Wu M, Zhao B H, Zong Y X. Analysis of world ginger production layout

and trade pattern. Northern Horticulture, 2019; 10: 141–150. (in Chinese)
[2] Wang W L, Zhang P C, Huang X P, Wang F Y. Comparative test of mechanical properties of typical ginger. Journal of Chinese Agricultural Mechanization, 2025; 46(12): 194–199. (in Chinese)
[3] Zhang P C, Jia S T, Wang F Y, Huang X P. Experimental study on mechanical properties of ginger plants. Journal of Chinese Agricultural Mechanization, 2024; 45(01): 117–121. (in Chinese)
[4] Zhang P C, Li F G, Wang F Y. Optimization and test of ginger-shaking and harvesting device based on EDEM software. Computers and Electronics in Agriculture, 2023; 213: 108257.
[5] Zhang J, Wang J, Du D D, Long S F, Wang Y W, Han C J, et al. Optimization and validation of root-cutting device for Chinese cabbage harvester based on discrete element method. Computers and Electronics in Agriculture, 2023; 214: 108314.
[6] Shaikh S A, Li Y M, Ma Z, Chandio F A, Tunio M H, Liang Z W, et al. Discrete element method (DEM) simulation of single grouser shoe-soil interaction at varied moisture contents. Computers and Electronics in Agriculture, 2021; 191: 106538.
[7] Makange N R, Ji C Y, Torotwa I. Prediction of cutting forces and soil behavior with discrete element simulation. Computers and Electronics in Agriculture, 2020; 179: 105848.
[8] Chen M D, Liu X T, Hu P X, Zhai X T, Han Z L, Shi Y L, et al. Study on rotor vibration potato-soil separation device for potato harvester using DEM-MBD coupling simulation. Computers and Electronics in Agriculture, 2024; 218: 108638.
[9] Wang Z D, Wang S S, Zhu P Y, Zhu D G. Research on key parameters of ginger rhizome excavation shovel based on discrete element method. Journal of Northwest A& F University (Natural Science Edition), 2025; 53(03): 124–136. (in Chinese)
[10] Chen G B, Wang Q J, Xu D J, Li H W, He J, Lu C Y. Design and experimental research on the counter roll differential speed solid organic fertilizer crusher based on DEM. Computers and Electronics in Agriculture, 2023; 207: 107748.
[11] Kim Y S, Siddique M A, Kim W S, Kim Y J, Lee S D, Lee D K, et al. DEM simulation for draft force prediction of moldboard plow according to the tillage depth in cohesive soil. Computers and Electronics in Agriculture, 2021; 189: 106368.
[12] Chen J X, He L N, Ou P Y, Han J R, Yue N B. Research on ginger cultivation techniques and pest and disease control measures. Seed Science & Technology, 2024; 42(22): 102–104. (in Chinese)
[13] Yu Y L, Xu L J, Yang H Q, Tan Z W, Dong W, Li H T, et al. Biological Characteristics and High-yielding and High-efficiency Cultivation Techniques of Ginger. Horticulture & Seed, 2021; 41(11): 30–32, 59. (in Chinese)
[14] Xu J S, Wu C C, Zhang N, Cao X. Research progress and prospects of ginger cultivation. Contemporary Horticulture, 2024; 47(13): 62–65. (in Chinese)
[15] Wang W C, Gao Q, Sun Y J, Wang N, Song Y M. Design and harvesting experiment of crawler self-propelled ginger harvester. Journal of Chinese Agricultural Mechanization, 2025; 46(10): 91–98, 106. (in Chinese)
[16] Jia B X, Sun W, Zhao Z W, Wang H C, Zhang H, Liu X L, Li H. Design and field test of a remotely controlled self-propelled potato harvester with manual sorting platform. American Journal of Potato Research, 2023; 100(3): 193–209.
[17] Li J W, Li X Y, Hu B, Gu T L, Wang Z J, Wang H L. Analysis of the resistance reduction mechanism of potato bionic digging shovels in clay and heavy soil conditions. Computers and Electronics in Agriculture, 2023; 214: 108315.
[18] Li J R. Potato-soil aggregate fragmentation and separation characteristics investigation. Inner Mongolia Agricultural University, 2023. (in Chinese) doi: 10.27229/d.cnki.gnmnu.2023.000511
[19] Wan L P C, Li Y L, Zhao H, Xu G H, Song J N, Dong X Q, et al. Gradient throwing characteristics of oscillating slat shovel for rhizome crop harvesters. Transactions of the CSAE, 2021; 37(24): 9–21. (in Chinese)
[20] Liu Y, Luo C M, Zong W Y, Huang X M, Ma L N, Lian G D. Optimization of clamping and conveying device for sunflower oil combine harvester header. Agriculture, 2021; 11(9): 859.
[21] Wang F Y, Qiu Z C, Pan Y F, Sun G Q. DEM-based parameter optimization and tests of digging green onions. Int J Agric & Biol Eng, 2023; 16(4): 126–133.
[22] Xiao X, Xie F P, Zhao Z Q, Wang X S, Liu D W, Zhao Y. Optimized design and experiment of the tassel gathering mechanism for 4BL-1 type white radish combine harvester. Transactions of the CSAE, 2024; 40(11): 38–47. (in Chinese)
[23] Wang Y M, Xue W L, Ma Y H, Tong J, Liu X P, Sun J Y. DEM and soil bin study on a biomimetic disc furrow opener. Computers and Electronics in Agriculture, 2019; 156: 209–216.
[24] Zhang Z H, Zhao L L, Lai Q H, Tong J. Operation mechanism analysis and experiments of shovel-type rolling soil-engaging components based on DEM-MBD coupling. Transactions of the CSAE, 2022; 38(15): 10–20. (in Chinese)
[25] Wang W L, Zhang D K, Wang X, Wang F Y. Parameter optimization and test of harvesting device for digging and pulling green onions based on discrete element analysis. Int J Agric & Biol Eng, 2025; 18(1): 165–172.
[26] Wang W L, Zhang P C, Wang X, Meng X J, Wang F Y. Construction of the particle simulation model for ginger-soil system using discrete element method. Int J Agric & Biol Eng, 2024; 17(5): 58–64.
[27] Zhang L, Zhai Y B, Wu C Y, Huang S Z, Zhang Z E. Modeling the interaction between a new four-bar subsoiling mechanism and red soil using the improved differential evolution algorithm and DEM. Computers and Electronics in Agriculture, 2023; 208: 107783.
[28] Tan H C, Shen C C, Ma J L, Wu C L, Xu L M, Ma S. The reduction of energy consumption and soil disturbance mechanisms in trenching using biomimetic blades. Computers and Electronics in Agriculture, 2025; 230: 109887.
[29] Tang H, Xu C S, Zhao J L, Wang J W. Stripping mechanism and loss characteristics of a stripping-prior-to-cutting header for rice harvesting based on CFD-DEM simulations and bench experiments. Biosystems Engineering, 2023; 229: 116–136.
[30] Wang J W, Xu Y N, Wang C Y, Xiang Y S, Tang H. Design and simulation of a trenching device for rice straw burial and trenching based on MBD-DEM. Computers and Electronics in Agriculture, 2023; 207: 107722.
[31] Lin J X, Liao Q X, Wang X F, Kang Y, Du W B, Zhang Q S. Exploring straw movement through the simulation of shovel-type seedbed preparation machine-straw-soil interaction using the DEM-MBD coupling method. Computers and Electronics in Agriculture, 2024; 226: 109465.
[32] Zeng Y, Jiang X H, Wu M L, Zhao Z H, Tang L W, Li P C. Development of the layered cut and throw ditching blade groups for oil tea forest based on DEM-MBD. Transactions of the CSAE, 2024; 40(08): 30–42. (in Chinese)
[33] Hou J L, Chen Y Y, Li Y H, Li T H, Li G H, Guo H E. Design and experiment of shovel-screen combined green onion digging, shaking, and soil tillage device. Transactions of the CSAE, 2021; 37(18): 29–39. (in Chinese)
[34] Hou J L, Li C, Lou W, Zhou K, Li Y H, Li T H. Design and test of floating clamping device for garlic combine harvester. Transactions of the CSAM, 2023; 54(01): 137–145. (in Chinese)
[35] Li H, He J, Wang Q J, Wang C, Wu Z Y, Guo Z Y. Analysis of slope-adaptive in covering-compacting device for no-till sowing based on DEM-MBD. Computers and Electronics in Agriculture, 2025; 233: 110175.
[36] Tang Z Y, Zeng Z W, Wu S L, Fu D B, He J H, Cai Y H, et al. Optimizing soil resistance and disturbance of bionic furrow opener for paddy field based on badger claw using the CFD-DEM method. Computers and Electronics in Agriculture, 2024; 227: 109549.
[37] Wang X Y, Lyu D Y, Ren J Y, Zhang M, Meng P X, Li X Q. Design and parameter optimization of the cleaning device for a bagged potato combine harvester. Transactions of the CSAE, 2022; 38(S1): 8–17. (in Chinese)
[38] Guan C S, Fu J J, Xu L, Jiang X Z, Wang S L, Cui Z C. Study on the reduction of soil adhesion and tillage force of bionic cutter teeth in secondary soil crushing. Biosystems Engineering, 2022; 213: 133–147.
[39] Wang Y, Zhang D, Yang L, Cui T, Jing H, Zhong X. Modeling the interaction of soil and a vibrating subsoiler using the discrete element method. Computers and Electronics in Agriculture, 2020; 174: 105518.
[40] Xie C S, Wei W B, Zhu Y J, Xiao M H, Chen T L. Wear reduction damage mitigation and operational reliability analysis of rotary tiller knives based on the self-excited vibration theory. Computers and Electronics in Agriculture, 2025; 231: 109991.